Trapped Brownian Motion in Single- and Two-Photon Excitation Fluorescence Correlation Experiments

Giuseppe Chirico,* Carlo Fumagalli, and Giancarlo Baldini

Dipartimento di Fisica, Istituto Nazionale per la Fisica della Materia, udr Milano-Bicocca, Piazza delle Scienze 3, I20126 Milano, Italy

Received: August 10, 2001; In Final Form: November 27, 2001

We investigate possible trapping effects induced by the infrared radiation employed for two-photon fluorescence spectroscopy and microscopy on the diffusion of small fluorophores and draw a comparison to single-photon excitation. A first-order treatment of the effect of an optical trapping potential on the diffusion time and the number of molecules per excitation volume is also derived. By analyzing the fluorescence fluctuations arising from solutions of small dyes versus the excitation power and comparing them to the results with microspheres, we show that the bias on the molecular diffusion of small dyes is negligible when two-photon excitation is employed. In single-photon excitation, close to the resonance absorption of the dye, a small but detectable bias effect on the diffusion is found, in agreement with the study by Osborne et al. [Osborne, M. A.; Balasubramanian, S.; Furey, W. S.; Klenerman, D. *J. Phys. Chem. B* **1998**, *102* (17), 3160].

1. Introduction

Two-photon excitation (TPE) fluorescence microscopy and spectroscopy was conceived more than 20 years ago[1,2] but has largely been developed in its modern form in the past decade.[3] It can be considered a comparatively young technique that takes advantage of both wide-field and confocal laser scanning microscopy (CLSM)[4,5] for the study of the three-dimensional (3-D) and dynamic properties of biological systems in vitro and in vivo.[6,7] A new type of spectroscopy related to the use of tiny excitation volumes has grown together with the development of confocal and two-photon excitation microscopy. The use of two-photon excitation microscopes has fostered the application of techniques such as fluorescence correlation spectroscopy (FCS)[8−11] or fluorescence lifetime (FL) to single biological molecules[12,13] and to the characterization of cellular environment[14,15] and tissues.[16] These applications have also been made possible by the development of mode-locked infrared (IR) lasers, which provide moderate average powers at high repetition rates with ultrafast pulses.[17] The use of infrared radiation in multiphoton experiments might affect the Brownian motion of the observed chromophores, and on the other hand, laser tweezers have been reported to induce two-photon excitation.[18] The main aim of the present report is to ascertain the extent to which the diffusion properties of small molecules of the size of simple dyes or small proteins (such as the green fluorescent protein) are affected by the use of pulsed IR radiation. This issue is particularly relevant for the investigation of dim fluorophores for which high excitation intensities should be used in two-photon experiments.

In fact, optical trapping is currently a valuable technique for the manipulation of microscopic objects ranging from a few tens of nanometers to a few micrometers in size. It is known[19] that electromagnetic radiation can apply a force on dielectric particles when strongly focused by a high-numerical-aperture objective.[20,21] Two types of forces act on the particles in this case: a gradient force that acts in the plane perpendicular to the light beam and is related the strength of the focalization of the laser beam and a scattering force that acts in the direction of the impinging light and is related to the scattering of the photons by the dielectric particle. The ratio of the two forces, which determines the stability of the trap, depends strongly on the wavelength ($\sim\lambda_0^5$), and the most stable traps have been developed in the infrared part of the light spectrum.[19] For molecules whose diameter $2a$ is less than the light wavelength (Rayleigh regime), the scattering force depends on the light intensity $I(r) = I_0 i(r)$ [with $i(0) = 1$], the refractive index of the medium n_m, and the particle polarizability α as[22]

$$|\bar{F}_{scat}| = \frac{8\pi^3 n_m}{3\epsilon_0 c \lambda_0^4}\alpha^2 I_0 \tag{1}$$

where ϵ_0, λ_0, and c are the vacuum dielectric constant, light wavelength, and speed of light, respectively. The gradient force depends on the gradient of the light intensity and the particle polarizability as[22,23]

$$\bar{F}_{grad} = \frac{n_m^2}{2c\epsilon_r\epsilon_0}\alpha\nabla\bar{I}(r) \tag{2}$$

where ϵ_r is the medium dielectric permittivity. The stability condition of the trap for a particle far from the absorption resonance is determined by the ratio of the gradient force to the scattering force that scales as[22]

$$\left|\frac{F_{grad}}{F_{scat}}\right| \propto \frac{\lambda_0^5}{\alpha w_0^2} \geq 1 \tag{3}$$

where w_0 is the waist of the laser beam. It is therefore easier to trap particles with infrared than with ultraviolet (UV) radiation, and the trapping of a dielectric particles depends on their size. Moreover, the trapping of small molecules might occur close

* Corresponding author: Giuseppe Chirico, Dipartimento di Fisica, Piazza delle Scienze 3, I20126 Milano, Italy. Tel.: 39-0264482872. Fax: 39-0264482894. E-mail: giuseppe.chirico@mib.infn.it.

10.1021/jp013087z CCC: $22.00
Published on Web 02/16/2002

to their absorbance resonance. Osborne et al.[24] reported biased diffusion of rhodamine 6G molecules for radiation at $\lambda = 514$ nm. They employed fluorescence correlation spectroscopy to measure the diffusion time through the excitation volume and detected an increase in diffusion time with increasing excitation power. We have argued that the nonresonant trapping of rhodamine is far too low to account for their findings and that the use of 514-nm argon laser radiation is more consistent with resonant trapping close to the absorption resonance of rhodamine.

The aim of this report is to determine the effect of IR radiation employed for two-photon excitation fluorescence experiments on the diffusion of the observed dye molecules. First, we extend the use of the fluorescence correlation methods applied by Osborne et al.[24] to characterize the trapping force induced by laser radiation by employing the photon-counting histogram method[25,26] and comparing it to the autocorrelation method. The trapping effect shows up as much in the diffusion time as in the number of molecules per excitation volume, which should increase with the excitation power. The diffusion time, however, is also affected by the distortion of the effective point spread function as a result of saturation of the dyes close to the laser focus, and we attempt to evaluate these two effects separately. One of the results of this report is to show that the detector response must be carefully characterized when the photon-counting histogram method is employed so that the number of particles per excitation volume can be estimated correctly, especially at low excitation powers. A second result of this report, derived in the Appendix, is an approximate theoretical treatment of the fluorescence correlation functions for Brownian particles diffusing in an optical trapping potential of small amplitude. This treatment is derived for the simple case of a 3-D Gaussian effective point spread function that describes, only qualitatively, the actual confocal excitation profile, and consequently, the analytical results given in the Appendix are essentially qualitative. However, these considerations support the interpolating functions used by us and by Osborne et al.[24] to describe the trend of the diffusion time and the number of particles per excitation volume versus the excitation power. Third, we compare the nonresonant trapping force induced by IR light ($\lambda \approx 770$ nm) on a small dye (rhodamine 6G) to the resonant trapping force induced by visible light ($\lambda = 532$ nm) close to the absorption resonance of rhodamine. In both cases, the trapping radiation also induces fluorescence emission, by either single-photon or two-photon absorption, and this is employed to characterize the diffusion by autocorrelation methods. The main result is to show that, for dyes and small proteins, the IR radiation used for two-photon excitation is not able to bias the Brownian diffusion appreciably whereas this effect can be detected when single-photon excitation is used. For small fluorescent microspheres, on the other hand, the diffusion is markedly affected by optical trapping and particle size, and these effects must be taken into account when the diffusion properties of these particles, which are often used as standards for excitation volume characterization, are derived.

2. Materials and Methods

2.1. Dye Solutions. Rhodamine 6G was purchased from Fluka (Fluka Chemika, catalog no. 83698), and a 100 μM stock solution was prepared in DMSO (dimethyl sulfoxide, Sigma Aldrich, catalog no. D-8779) and kept at 4 °C in the dark. All dilutions were prepared in bidistilled MilliQ (Millipore Inc.) water from the same stock. The concentrations of the stock and of the samples were checked spectrophotometrically, using an extinction coefficient of $\sim$92 000 M^{-1} cm^{-1} in DMSO at $\lambda =$ 524 nm (Molecular Probes, Eugene, OR). The concentrations of the samples investigated here range between 250 and 0.5 nM. The concentrations of the more-dilute samples were determined by known dilutions of a sample whose concentration was measured. Fluorescein was purchased from Fluka (Fluka Chemika, catalog no. 46955), and a 100 μM stock solution was prepared in TRIS buffer (10 mM, pH = 8.2) and kept at 4 °C in the dark. All of the samples were prepared by dilution of the stock with the same TRIS buffer prepared from bidistilled MilliQ (Millipore Inc.) water. The concentrations of the stock and of the samples were checked spectrophotometrically, using an extinction coefficient of $\sim$75 000 M^{-1} cm^{-1} at $\lambda = 492$ nm (Molecular Probes, Eugene, OR).

2.2. Microsphere Suspensions. Yellow-green fluorescent latex microspheres of diameter 64 $\pm$ 9 and 209 $\pm$ 12 nm (Polysciences, Fluoresbrite YG, catalog no. 17149) were suspended in deionized and filtered (0.22 μm, Millipore filter) water, and all concentrations were determined by dilution from the mother solution, which was 2.6% in solid content, corresponding to $\sim$400 nM. After the 64-nm microsphere solutions had been filtered with a 0.22-μm Millipore filter and the 209-nm microsphere solutions with a 0.45-μm Millipore filter, the samples were loaded into one of the eight plastic wells mounted on the top of a 0.17-μm glass slip (Nalgene-Nunc, Rochester, NY) sample holder and measured at room temperature. The concentrations were checked spectrophotometrically by preparing a solution at $C = 40$ nM by weight dilution from the stock. The absorption extinction coefficient was measured on this sample with elimination of the scattering contribution. The absorption spectrum measured by the spectrophotometer was fit to an inverse fourth power law dependence in the range $550 < \lambda < 650$ nm, where no contribution form the excitation of the dye is expected. The correct spectrum was then obtained by subtraction of this scattering contribution from the measured absorption spectrum. The concentrations of all of the samples used here were determined by comparison with this reference spectrum after the scattering contribution has been taken into account.

2.3. Single-Photon Setup. The single-photon setup was built around an inverted microscope (TE300, Nikon, Tokyo, Japan); the excitation light was provided by a solid-state laser at 532 nm and 2 W (Millennia II, Spectra Physics, Mountain View, CA). The laser light was reflected by a dichroic mirror (530DCSPRX, Nikon, Tokyo, Japan) and focused on the sample with a 100$\times$ oil objective (numerical aperture, NA = 1.4, Plan Apochromat DICH 100$\times$ oil, working distance = 0.19 mm, focal length = 2 mm, Nikon, Tokyo, Japan). The fluorescence light was detected through a band-pass filter (HQ560/30, Chroma, Brattleboro, VT) by a Hamamatsu R464 photomultiplier for single-photon counting, and the signal was digitized by a C3866 Hamamatsu photon-counting unit. The fluorescence light was filtered by a 100-μm pinhole set at the image plane of the TE300 side port. In this way, the effective excitation volume as measured by fluorescence correlation methods on dilute fluorescein solutions was $V_{exc} = 0.6 \pm 0.01$ fL (1 fL = 1 μm^3). The excitation power was measured with a photodiode (ThornLab, North Newton, NJ, model Det210) right on the sample plane. All measurements reported here were performed at a temperature of 24° C.

2.4. Two-Photon Setup. The optical setup was based around an inverted microscope (TE300, Nikon, Tokyo, Japan); the excitation light was provided by a mode-locked Ti:sapphire laser (Tsunami 3960, Spectra Physics, Mountain View, CA) pumped by a solid-state laser at 532 nm and 5 W (Millennia V, Spectra

Physics, Mountain View, CA). In this configuration, the Ti:sapphire laser generates a pulsed source with a maximum of ~700-mW average power output at $\lambda = 770$ nm, 100-fs full width at half-maximum, and 80-MHz repetition frequency. The laser light was reflected by a dichroic mirror (650 DCSPRX C72-38, Nikon, Tokyo, Japan) and focused on the sample with a 100× oil objective (NA = 1.4, Plan Apochromat DICH 100× oil, working distance = 0.19 mm, focal length = 2 mm, Nikon, Tokyo, Japan). The fluorescence emission was collected by the same objective and passed through the dichroic mirror and through a band-pass filter (HQ535/50, Chroma, Brattleboro, VT) to diminish the red and infrared light reflected toward the detector. The laser was steered for ~2 m on the optical bench so that the entrance pupil of the objective was approximately filled, and the excitation volume measured by fluorescence correlation[27] was $V_{exc} = 0.17 \pm 0.04$ fL. The excitation power on the sample was approximately one-third of the power entering the objective, whose transmission was ~80% for $\lambda = 770$ nm. All measurements reported here were performed at $\lambda = 770$ nm and at a temperature of 22 °C.

2.5. Data Analysis. The acquisition of the photon counts was performed by an 80-MHz digital card from ISS (ISS, Urbana-Champaign, IL). All of the measurements reported here were acquired at a 20-kHz sampling frequency and, when not stated otherwise, for 2×10^6 total samples. The correlation functions and the histograms were computed on-line by the card.

The fluorescence fluctuations can be characterized by two alternative and complementary methods. We can compute the autocorrelation function (ACF) of the fluctuations of the fluorescence signal $\delta F(t) = F(t) - \langle F \rangle$

$$g(t) = \langle \delta F(t)\, \delta F(0) \rangle / \langle F(0) \rangle^2 \tag{4}$$

The average of the square of the fluorescence fluctuation, $g(0) = \langle \delta F^2(0) \rangle$, is related to the average number concentration C by

$$g(0) = \xi / (V_{exc} C) \tag{5}$$

where the factor ξ depends on the type of excitation,[10] with $\xi_{1p} = 0.5^{3/2}$ and[14] $\xi_{2p} \approx 0.076$ for one- and two-photon excitation, respectively. For the case of single-photon excitation, the volume of the excitation profile is determined by the laser beam waist, w_0, and by the depth of focus, z_0, of the spatial filtering setup as $V_{exc} = (\pi/2)^{3/2}\, w_0^2 z_0$, whereas for the case of two-photon excitation, $V_{exc} = \pi w_0^4 / \lambda$.

The autocorrelation functions are

$$g_{1p}(t) = g_{1p}(0)(1 + t/\tau_{1p})^{-1}[1 + t/(\zeta \tau_{1p})]^{-0.5} \tag{6}$$

and[14,27]

$$g_{2p}(t) = g_{2p}(0)(1 + t/\tau_{2p})^{-1} \tag{7}$$

for the single- and two-photon cases, respectively. The relaxation time is related to the translational diffusion coefficient D of the fluorophore by[10] $\tau_{1p} = w_0^2/(4D)$ and[27] $\tau_{2p} \approx 1.15 w_0^2/(8D)$. The volume depth for the single-photon excitation case is accounted for by the factor ζ, which, for our single-photon setup, can be estimated[28] as $\zeta \approx 25$.

The ACFs were analyzed by means of custom-coded least-squares fitting programs based on the Marquardt algorithm[29] using the routine MRQMIN[30] for fitting. From the analysis of the ACFs, we obtain the relaxation time τ and the zero-lag-time term $g(0)$. As discussed later, the measurements of the fluorescence fluctuations in rhodamine 6G solutions at various concentrations and low excitation power provides an estimate of the laser beam waist, w_0, once a value for the translational diffusion coefficient of $D \approx 280\ \mu m^2/s$ is assumed at $T = 22$ °C.[28,31]

The fluorescence fluctuations can also be characterized by computing the histogram of the photon counts. For a stable source, we expect a Poisson distribution because of the random behavior of the emission of the photoelectrons by the detector photocathode. On the other hand, the distribution of the fluorescence photon counts collected from a small volume of a fluorophore solution is known to be super-Poissonian.[25,26,32] From the first two moments of the histograms, we can obtain the average number of molecules in the excitation volume N and the molecular brightness ϵ, a parameter that is proportional to the fluorophore quantum yield times the cross section

$$\begin{aligned} \langle k \rangle &= N\epsilon \\ Q &= \frac{\langle k^2 \rangle - \langle k \rangle^2}{\langle k \rangle} - 1 = \xi \epsilon \end{aligned} \tag{8}$$

It is worth noting that the above equations are valid for any form of the point spread function, as shown for a single-component solution in the Appendix. Obviously, the numerical value of ξ is related to the shape of the point spread function. For a Poisson distribution of photon counts, $Q = 0$, whereas for the case of interest here, $Q > 0$. The analysis provided in the following paragraphs is based on the evaluation of N and ϵ from the inversion of eq 8.

3. Results

3.1. Effect of Detector Response on Photon Statistics. It is our aim to characterize the effect of the trapping force induced in FCS experiments by studying the trend of the diffusion time of the particles in the excitation volume versus the excitation intensity. The fluorescence is excited by the same laser light that traps the fluorescent particles. In addition to the autocorrelation methods already employed,[24] we want to exploit the recently developed photon-counting histogram method.[25,26,32] It is therefore essential to investigate accurately the possibility of artifacts being present in the signal as a result of being induced by either the detector electronics or the internal photodynamics of the fluorophores. We investigated the response of the detectors by studying their response to a stable light source, a DC-biased LED (light-emitting diode). For a stable source, the photon-counting histogram should be well described by a Poisson curve. However, for the photomultiplier and the avalanche photodiode used here, we found that the histograms of the photon counts k show a systematic deviation from a Poisson curve characterized by $Q > 0$. In the case of the photomultiplier, this effect depends on the anode−cathode bias, as shown in Figure 1 (upper panel). For the avalanche photodiode, we studied the histograms of the photon counts versus the bias of the LED. The result is shown in Figure 1 (lower panel), where we report both the average number of photon counts and the Q factor versus the LED bias. The average value is $\langle Q \rangle = 0.011 \pm 0.0004$ for the avalanche photodiode, which is to be compared with the minimum value obtained for the photomultiplier, $Q_{PMT} \approx 0.005 \pm 0.000\,05$. The use of a photomultiplier at the optimum cathode−anode bias should therefore be advantageous in terms of the Q factor. However the very low noise equivalent power (NEP $\leq 10^{-15}$ W) of the APD allows for the detection of fluorescence from highly diluted

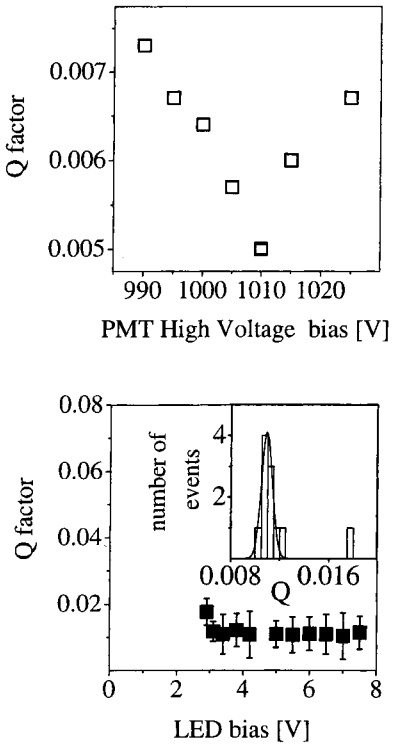

Figure 1. Characterization of the detectors. Upper panel: Q factor of the histograms of the photon counts detected by the photomultiplier from a DC-biased LED versus the pmt voltage. Lower panel: Characterization of the avalanche photodiode response. The source is a green LED biased with a DC voltage in the range of 2−8 V. The Q factor is shown versus the LED bias. The inset of this panel shows the distribution of the Q values obtained for all LED bias values.

solutions with larger fluorescence fluctuations. At the moment, we have no simple rationalization for the intrinsic Q factors determined for the two detectors. It is likely that the presence of a small fraction of afterpulses would enhance the probability of counting larger numbers of photons and would deform the photon-counting histogram toward the higher counts in a way that corresponds to $Q > 0$.

It is therefore important to correct the data for the intrinsic Q factor of the detectors mainly for low fluorescence rates that might correspond to highly diluted solutions, low excitation powers, or dim fluorophores. It must be noticed that the use of high excitation powers might induce additional fluctuations through the internal photodynamics of the fluorophore (triplet state, higher-order excitations).[33] Therefore, one should try to use the lowest excitation power possible to minimize unwanted effects in the fluorescence fluctuations. It is easy to see from eqs 8 that the Q factor due to the detector, Q_D, would induce an overestimate of ϵ and therefore an underestimate of N. If we assume that the detector fluctuations are decoupled from the fluorescence fluctuations, we can modify eqs 8 to read

$$\begin{aligned} \langle k \rangle &= N\epsilon \\ Q - Q_D &= \xi\epsilon \end{aligned} \tag{9}$$

3.2. Effect of Excitation Power on Fluorescence Fluctuations. We first verified the assumption made in eqs 9 with simple two-photon experiments on fluorescein solutions in water at a concentration $C \approx 20$ nM versus the excitation power. The measurements were performed at excitation powers in the range 3−30 mW and at $\lambda = 750$ nm. The autocorrelation functions were analyzed as described in the Data Analysis section, and

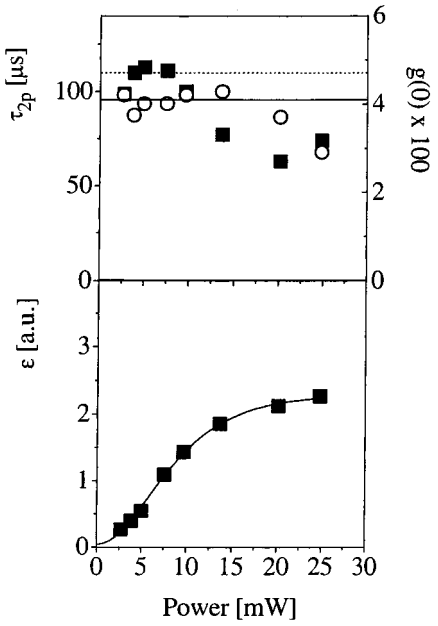

Figure 2. Results of the analysis of the autocorrelation functions for a solution of fluorescein at pH ≈ 8 and $C = 20$ nM at increasing excitation powers in two-photon excitation at $\lambda = 750$ nm. Upper panel: Relaxation time τ_{2p} (left axis, ■) and $g(0)$ (right axis, ○). The dashed and solid lines indicate the average values of $\tau_{2p} = 110 \pm 12$ μs and $g(0) = 0.04 \pm 0.002$ over the four lowest excitation powers. Lower panel: Fluorescence molecular brightness, ϵ, versus the excitation power. The solid line is a fit of the data to the function $\alpha P^2/(1 + \beta P^2)$.

the photon-counting histograms were analyzed according to eqs 9. The result of the autocorrelation function analysis is reported in Figure 2, together with the trend of the fluorescence count rate versus the excitation power. As we verified previously using the same setup for labeled microspheres,[27] the fluorescence count rate scales with the square of the excitation power for low excitation intensities. In the present case, where we extend to larger powers, we observe that the fluorescence increases quadratically for low excitation powers and then levels off at larger excitations powers, probably as a result of higher excited states.[31] At the same time, the relaxation time and the initial fluctuation $g(0)$ decrease with the excitation power. The average values obtained for the four lowest powers are $\tau_{2p} = 110 \pm 10$ μs and $g(0) = 0.041 \pm 0.002$, and the power at which τ_{2p} and $g(0)$ start to decrease from these average values is close to the power at which the fluorescence count rate rounds off. The value of the relaxation time corresponds to a beam waist $w_0 = 0.46 \pm 0.02$ μm when a diffusion coefficient value of $D = 280$ μm^2/s is assumed. This value leads to an excitation volume of $V_{exc} = 0.19 \pm 0.03$ fL, which is compatible with our previous estimate of the excitation volume,[27] $V_{exc} = 0.17 \pm 0.04$ fL. The value of $g(0)$ corresponds to an average number of molecules in the excitation volume $N = 1.8 \pm 0.09$. By assuming $V_{exc} = 0.17 \pm 0.04$ fL, we can compute a concentration of $C = 18 \pm 4$ nM, which is close to the nominal value.

Using the same measurements, we computed the first two moments of the photon-counting distribution to obtain the molecular brightness and the average number of molecules per excitation volume. We compared the two sets of equations, eqs 8 and 9, and obtained the molecular brightness ϵ, from which we then computed the average number of molecules N. A comparison of the two types of computation is displayed in Figure 3. We observe that, when no account is made of the intrinsic Q factor, Q_D, the average number of molecules increases steadily with the excitation power, especially for very

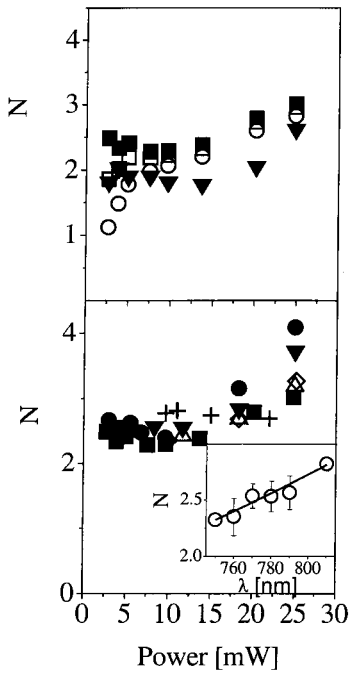

Figure 3. Average number of molecules per excitation volume as obtained from the analysis of the photon-counting histograms of the two-photon excitation experiments on fluorescein solutions at increasing excitation powers and at $\lambda = 750$ nm. Upper panel: ■, $N = \langle k \rangle/(\epsilon - 0.145)$; ○, $N = \langle k \rangle/\epsilon$; □, $N = \langle k \rangle/(\epsilon - 0.105)$; ▼, $N = g(0)/0.076$ obtained from the analysis of the autocorrelation functions (see Figure 2). The solid lines are only a guide to the eye. Lower panel: Results of the analysis of the photon-counting histogram, $N = \langle k \rangle/(\epsilon - 0.145)$, for different excitation wavelengths. ■, $\lambda = 750$ nm; ◇, $\lambda = 760$ nm; ●, $\lambda = 770$ nm; △, $\lambda = 780$ nm; ▼, $\lambda = 790$ nm; +, $\lambda = 810$ nm. Inset of lower panel: Average number of molecules averaged over the lowest four excitation powers versus the excitation wavelength. The solid line is a force fit to a cubic power law, whereas the dashed line is the best-fit power law, which corresponds to an exponent of ~2.7.

low powers (see open circles in Figure 3 upper panel), contrary to what is expected and found when eqs 9 are employed. In Figure 3, we also report the values of the average number of molecules obtained from the initial value of the ACF, $g(0)$, as $N_{g(0)} = 0.076/g(0)$, which is found to be slightly lower than the values obtained by inverting eqs 9. Moreover, for larger excitation powers, corresponding to the departure from the square-law dependence of the fluorescence count rate (see Figure 2, lower panel), we observe an increase in the effective average number of molecules for all types of analysis performed. A computation of the fluorescein concentration from the average number of molecules computed over the four lower excitation power points in Figure 2, as done for $N_{g(0)}$, gives $C = 22 \pm 5$ nM. Finally, as a further check on the measurement of the average number of molecules in the excitation volume, we considered the dependence of N on the excitation wavelength. The inset of the lower panel of Figure 3 reports the experimental values obtained from an average for powers of ≤10 mW versus the excitation wavelength. The dependence is close to the expected cubic-law dependence (solid line), as the best-fit power law corresponds to an exponent of ~2.7 ± 0.3.

3.3. Single-Photon Experiments on Rhodamine versus Power. We first tested the effect of the excitation power on rhodamine diffusion by performing measurements of the fluorescence fluctuations from dilute rhodamine solutions (at $C = 70$ nM) versus the excitation power in the range 300−900 μW with single-photon excitation at $\lambda = 532$ nm. The fluctuations were characterized by the PCH and FCS methods

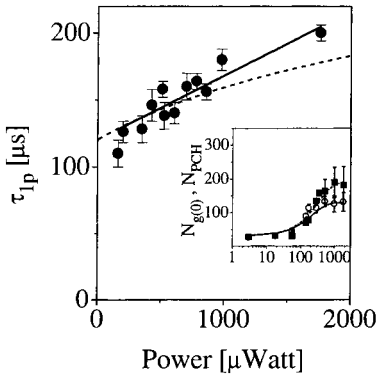

Figure 4. Relaxation time τ_{1p} of the ACFs of single-photon excitation fluorescence from rhodamine 6G solutions at $C = 70$ nM versus the excitation power. The solid line is a linear fit of the data, and the dashed line is the prediction made according to the saturation effect as discussed in the text. Inset: Average number of molecules obtained from the $g(0)$ value, $N_{g(0)}$ (○) and from the PCH analysis, N_{PCH} (■). The solid and dashed lines are fits to eq 13 of the text.

to determine the average number of molecules N and the diffusion time τ_{1p} of the molecules through the excitation volume. The average number of molecules shown in Figure 4 increases at first linearly with excitation power and reaches a plateau at powers of ~500 μW. The extrapolation to vanishing powers is $N = 26 \pm 4$, which for an excitation volume of $V_{exc} = 0.6 \pm 0.01$ fL, corresponds to a concentration of 72 ± 7 nM, in close agreement with the nominal value. The relaxation time τ_{1p} increases with the excitation power, and the trend is well approximated by a linear law

$$\tau = \tau_0\left(1 + \frac{u}{KT}P\right) \tag{10}$$

with $u = 0.015 \pm 0.004$ eV/mW and $\tau_0 = 120 \pm 6$ μs. The value of the relaxation time leads to a beam waist of $w_0 = 0.38 \pm 0.02$ μm if a diffusion coefficient of $D \approx 300$ μm²/s at $T = 24$ °C is assumed.

The average number of molecules obtained from an analysis of the histograms and ACFs is reported in the inset of Figure 4. The lines are best-fit curves to an equation of the type of eq 57 derived in the Appendix and discussed later.

3.4. Two-Photon Experiments on Rhodamine versus Power. We studied the effect of infrared excitation on the diffusion properties of rhodamine molecules in solutions at $C = 5$ nM. The rhodamine fluorescence is excited at $\lambda = 760$ nm, and the emission is selected by a 535-nm band-pass filter (40-nm full bandwidth). The fluorescence fluctuations were characterized by the PCH and FCS methods. The first two moments of the photon counts increase with the excitation power though with a slight roll off at large excitation powers as shown in the inset of Figure 5. However, the number of molecules obtained from eqs 9 does not show a systematic trend versus the excitation power, and the change observed for the first two moments is due only to the change in the molecular brightness. The average value of N obtained from Figure 5 is $N = 0.43 \pm 0.06$, which corresponds to a concentration of $C = 4.3 \pm 1$ nM, in good agreement with the preparation of the solution. For the FCS analysis, the relaxation time of the ACF does not show an appreciable dependence on the power, as shown in the inset of Figure 5. The average value of the relaxation time is $\tau_{2p} = 87 \pm 8$ μs, which, assuming $D = 300$ μm²/s for rhodamine, corresponds to an excitation volume for the two-photon excitation of $V_{exc} = \pi w_0^4/\lambda = 0.18 \pm 0.03$ fL, in good agreement with the values previously determined for this setup.[27]

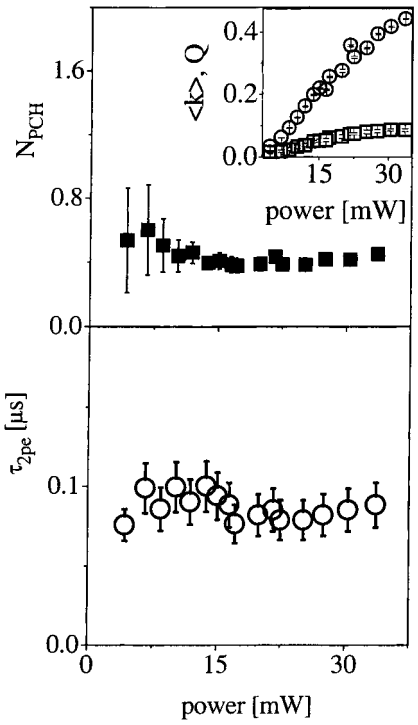

Figure 5. Results of the analysis of the ACF of two-photon excitation fluorescence from rhodamine 6G solutions at $C = 5$ nM versus the excitation power. Upper panel: Number of molecules per excitation volume versus the excitation power. The data were obtained from a PCH analysis of the raw photon-counting data. Inset: First momentum, $\langle k \rangle$, and Q factor versus the excitation power. Lower panel: Relaxation time of the ACF.

3.5. Two-Photon Experiments on Microspheres versus Power. We then investigated the fluorescence fluctuations of highly diluted fluorescent microsphere (64 nm in diameter) solutions at wavelengths of $760 < \lambda < 800$ nm and at increasing excitation powers. The concentration of the solution is $C = 115$ pM. The data were collected at a 20-kHz sampling frequency, and the ACFs were computed over 1.6-s-long buffers. The fluorescence fluctuations are notably high because of the low concentrations, as is evident from the spread on the ACFs collected at ~7 mW of excitation power on the 64-nm microsphere solution (see inset of Figure 6). An analysis of these ACFs gives a distribution of relaxation times, as shown in Figure 6, where the average values of the relaxation time and $g(0)$, shown with a vertical arrow, occur at values slightly larger than the center of the Gaussian fit. As the excitation power increases, the discrepancy between the center of the Gaussian fit and the average value of the two quantities grows larger, as shown in Figure 7. Very similar behavior is found for the 209-nm microspheres, as shown in the lower panel of Figure 7.

4. Discussion and Conclusions

We have compared the effect of the excitation intensity on the diffusion properties of a small dye for single- and two-photon excitation. The relaxation time of the ACFs increases with increasing power for single-photon excitation, whereas for two-photon excitation, no appreciable dependence is found. The relaxation times extrapolated to zero power are compatible with the known excitation volumes for the two setups. Moreover, the average number of molecules per excitation volume increases with excitation power, reaching a plateau for single-photon excitation and remaining remarkably constant for two-photon excitation. In the Appendix, we derive a simple approximate

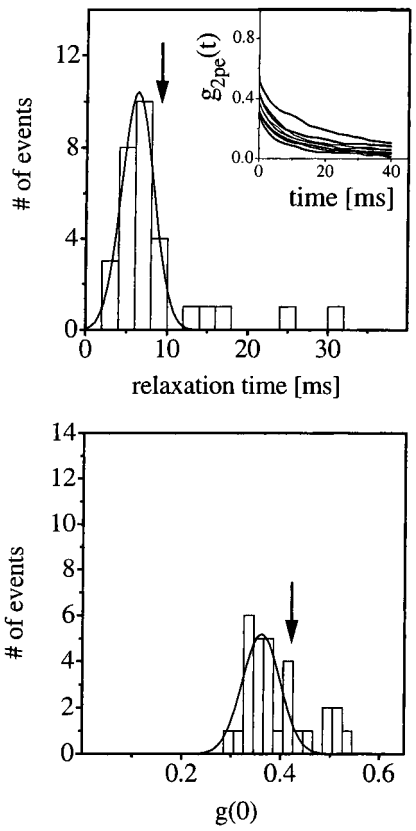

Figure 6. Results of the analysis of the ACFs computed over contiguous 1.6-s buffers for a 125 pM solution of 64-nm microspheres at $P \approx 7$ mW. Upper panel: Distribution of best-fit relaxation times. Lower panel: Distribution of the best-fit $g(0)$ values. The vertical arrows indicate the average values. In the inset, some of the ACFs are shown.

expression for the ACF of the fluorescence in the presence of a small optical trapping potential. The result, to first order in the potential, is that the relaxation time and the average number of molecules increase linearly with the optical trapping potential. These equations have also been assumed in other works.[24] In the following, we analyze the trends of the relaxation times and number of molecules according to these relations.

The results shown in Figure 4 suggest that the use of single-photon excitation at a wavelength close to the absorbance resonance of the dye biases the Brownian motion, thus hindering the diffusion. From the slope determined in Figure 4, $u = 0.015 \pm 0.005$ eV/mW, we can estimate the molecular polarizability. As shown in the Appendix, the slope of the diffusion time with the excitation power (see eq 10) is given approximately by

$$u\ (\text{eV/mW}) = \frac{n_m \alpha}{2} \frac{n_m}{\epsilon_0 \epsilon_r c(\pi {w_0}^2/2)} \times 6.25 \times 10^{18} \quad (11)$$

where n_m and ϵ_r are the medium refraction index and dielectric permittivity, respectively ($n_m = 1.33$, $\epsilon_r \approx 80$). From a comparison of the experimental data to eq 11, we estimate a value for the polarizability of $\alpha = 0.58\ (\pm 0.15) \times 10^{-33}$ m^3 for rhodamine 6G at $\lambda = 532$ nm. From a theoretical point of view, the polarizability of a particle that is sufficiently small that the instantaneous electric field can be considered constant over the particle volume can be approximated by the Clausius−Mossotti law[34]

$$\alpha = 4\pi\epsilon_0 {n_m}^2 r^3 \left(\frac{m^2 - 1}{m^2 + 2}\right) \quad (12)$$

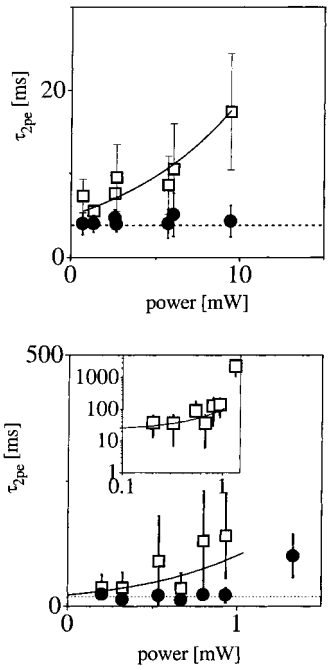

Figure 7. Summary of the analysis of the ACFs for microsphere solutions: upper panel, 64-nm microspheres; lower panel, 209-nm microspheres; □, average values of the relaxation times; ●, center of the Gaussian fit of the distribution of the relaxation times; - - -, expected relaxation time computed from the solution viscosity and the microsphere diameter (see text); —, best linear fits of exponential growth to the data.

where n_p is the refractive index of the particle, m is the ratio n_p/n_m, and r is the effective particle radius. By assuming, for example, $r = 1$ nm, $n_p = 1.6$, and $w_0 \approx 0.4$ μm ($V_{exc} = 0.6$ fL, $z_0/w_0 \approx 5$) for the single-photon excitation in our setup, we estimate a value of $\alpha \approx 1.6 \times 10^{-37}$ m^3, which is almost 4 orders of magnitude lower than the experimental estimate made by analyzing the slope of a plot of the diffusion time versus the excitation power. A similar discrepancy was obtained by Osborne et al.[24]

When treating the relaxation time of the autocorrelation function, we must also take into account the saturation effects that result in a perturbed point spread function. The molecules closer to the focus of the laser suffer partial saturation as a result of the high laser intensity, and the number of molecules that emit fluorescence is therefore less than expected for the ideal case when no saturation occurs. By following the theoretical and experimental work of Widengren et al.,[35] we estimated for rhodamine 6G the ratio between the excited-state population S_1 and the ideal population that one would obtain in the absence of saturation effects. The ratio goes from ~0.76 at $P = 300$ μW to ~0.52 at $P = 900$ μW, indicating that substantial saturation effects are present already at these powers. We estimated the change in the diffusion time of the autocorrelation function by fitting the excited-state population distribution $S_1(\bar{r}, z)$ to a Gaussian profile of the type $\exp[-2r^2/w(P)^2]$ in the plane $z = 0$. The relaxation time was then computed versus the excitation power as $\tau(P) = w(P)^2/(4D)$, and the result is reported in Figure 4 as a dashed line. These considerations confirm that the ground-state saturation has a considerable effect on the relaxation time, although not all of the observed rise can be explained in this way. A quantitative evaluation of the polarizability should therefore also take this effect into account, which would lead to a smaller value that, in any case, would be far larger than the one predicted by the simple Clausius−Mossotti law.

An independent measure of the bias on the Brownian diffusion can be obtained from an analysis of the dependence of N on the excitation power. The probability that the Brownian particle diffuses out of the trapping potential well is proportional to the Boltzmann factor, $\exp(-\Delta U/KT)$, where $\Delta U = U_\infty - U_{min}$ is the difference between the potential far from the optical trap, U_∞, and the potential in the minimum of the optical trap, U_{min}. Therefore, the difference between the observed (N_{obs}) and unbiased (N_0) numbers of dyes in V_{exc} can be written as

$$N_{obs} = N_0 + A\left[1 - \exp\left(-\frac{uP}{KT}\right)\right] \qquad (13)$$

The simple approximate treatment given in the Appendix suggests that the parameter A, used here as a simple fitting parameter, should be related to the shape of the light excitation profile. The solid and dashed lines in the inset of Figure 4 are the best fit to eq 13, which gives values of $u = 0.03 \pm 0.01$ and $A = 130 \pm 40$. The value of u is higher than the corresponding estimate made by fitting the relaxation times, although it is almost within the experimental uncertainty in the data. The average of the estimates of the trapping potential obtained from the diffusion time and from the number of particles leads to $u = 0.023 \pm 0.008$ eV/mW. Osborne et al.[24] measured $u = 0.08 \pm 0.04$ eV/mW, a value ~4 times larger than the present estimate. One of the causes for this difference could be the beam waist, w_0, of the setup used by Osborne, who reported[24] $w_0 = 0.528 \pm 0.042$ μm. However, this value is similar to that estimated for our setup, $w_0 \approx 0.4$ μm, and by taking eq 11 into account, our estimate of u should be multiplied by a factor ~0.6 to be compared to the estimate made by Osborne et al., which leads to an even larger discrepancy. A second possible explanation for the observed difference could be in the polarizability value for rhodamine 6G, as we are exciting at $\lambda = 532$ nm whereas Osborne et al.[24] employed the line at $\lambda = 514$ nm. These two wavelengths flank the main peak of rhodamine 6G absorption in water, which has a maximum at $\lambda \approx 524$ nm.

The value of the best-fit parameter A indicates an increase in the average number of particles by a factor of 5 ± 0.5. The factor predicted by the simple first-order treatment given in the Appendix for the 3-D Gaussian case, ~0.2, is much lower than our experimental estimate. The increase in N with excitation power computed from a linear fit of the three lowest values of the excitation power is ~3, closer to the theoretical value although still larger. This discrepancy might be due to the crude approximations used in the computations reported in the Appendix, particularly the assumption of a 3-D Gaussian excitation profile.

From these single-photon experiments, we therefore find a several order of magnitude discrepancy between the experimental estimate of u and the prediction made on the basis of the Clausius−Mossotti law, and it seems reasonable to ascribe this discrepancy to the presence of resonant optical trapping, as done by Osborne et al.[24] Unfortunately, we are not aware of any direct measurement of α for rhodamine close to resonance, and the use of eq 12 for a simple molecule treated as a dielectric is questionable. Equation 12 does not apply to the resonance case, and the assumption of a refraction index, $n_p = 1.6$ in our case, probably has no meaning for such a small scale. At present, we have no simple and direct explanation for the discrepancy, and therefore we suggest, as did Osborne et al.,[24] that the

observed power dependence is due to the resonantly large polarizability of rhodamine.

On the other hand, the analysis of the two-photon excitation experiments reported in Figure 5 clearly shows that the relaxation time and the average number of molecules have no evident dependence on the average excitation power. This is in good agreement with the theoretical estimate for the nonresonant case, $u \approx 10^{-7}$ eV/mW, as such a slope could not be measured with the present experimental accuracy. We conclude therefore that the two-photon FCS experiments are less affected by possible optical bias of the Brownian diffusion than the conventional confocal single-photon measurements.

However, the possibility of optical trapping in two-photon FCS experiments must be taken into account when larger particles are investigated. The experiments on two sets of microspheres reported in Figure 6 indicate that, in some instances, the microspheres experience a retarded diffusion. At the highest excitation powers, the histograms show a peak at low relaxation time and few events corresponding to large relaxation times. The main peak can be fit to a Gaussian curve (Figure 6), and the center of the Gaussian, τ_G, remains relatively constant with increasing excitation power, as shown in Figure 7. The values averaged over the entire set of excitation powers are $\tau_G = 4.3 \pm 0.4$ and $\tau_G = 19 \pm 5$ ms for the 64- and 209-nm microspheres, respectively. The theoretical estimate of the diffusion times for these particles, whose size is comparable to the beam waist, can be made by also taking into account the particle radius, R, according to the relation[38] $\tau_{2p} = (w_0^2 + R^2)/(8D)$. The theroretical estimates made for $T = 22$ °C, $w_0 = 0.45 \pm 0.03$ μm, and $\lambda = 770$ nm are $\tau_{2pe} = 3.8 \pm 0.4$ ms for the 64-nm microspheres and $\tau_{2pe} = 13.1 \pm 1.4$ ms for the 209-nm microspheres, in good agreement with the averages of the centers of the Gaussian fits τ_G. In addition, the contribution of the particle size to the diffusion time, $R^2/(8D)$, amounts to 0.02 ms for the 64-nm beads and 0.67 ms for the 209-nm beads. This indicates that the main component of the distribution is due to microspheres that experience free Brownian diffusion. On the other hand, the arithmetic averages of the relaxation times increase with the excitation power. For the 64-nm microspheres, the trend is linear over the entire range of excitation powers, whereas for the larger microspheres, the relaxation time seems to increase more rapidly for excitation powers of ≥ 1 mW, as shown in the inset of Figure 7, where the solid curve corresponds to a linear relation. The slopes that can be estimated in the linear region are 0.7 ± 0.05 and 30 ± 9 ms/mW for the 64- and 209-nm microspheres. We expect the slopes to be proportional to the trapping potential and, therefore, to the polarizability α, which scales as the particle volume (see eq 12). In fact, the slope for the larger microspheres is sensibly larger than that observed for the 64-nm microspheres, and the ratio of the slopes determined from Figure 7 is $\sim 43 \pm 13$, which is close to the ratio of the volumes of the two microspheres ($\sim$35). This agreement is also remarkable because of the use of the Clausius−Mossotti relation for particles that are not much smaller than the light wavelength. Moreover, the presence of the larger microspheres in the excitation volume might lead to some deformation of the laser profile, and this would affect the trapping properties.

In conclusion, we have observed a power dependence of the diffusion times and average numbers of particles N_{exc} for a small dye excited at a wavelength close to its absorbance resonance. This behavior can be ascribed to resonant optical trapping, as was done by Osborne et al.,[24] and it must be taken into account when accurate measurements of the diffusion coefficients by single-photon FCS methods are needed. For two-photon excitation, no appreciable dependence is observed for rhodamine, in agreement with the expected optical trapping potential. This behavior should facilitate the estimation of the diffusion coefficient of small fluorophores from an analysis of the fluorescence fluctuations when two-photon excitation rather than conventional single-photon excitation is used. This advantage can be extended to the study of small proteins (typically 2−10 nm in diameter) whose polarizability should be sufficiently low in the IR region to not induce optical trapping. In fact, we have verified that, when microspheres are employed, a small but appreciable effect on the relaxation time of the correlation functions is already observed for microspheres of the size of approximately 60 nm. Optical trapping effects with two-photon IR excitation should therefore affect only negligibly the diffusion of most proteins whose sizes are on the order of a few nanometers.

Acknowledgment. This work was partially supported by the PAIS SingMol of the Istituto Nazionale per la Fisica della Materia (INFM). We are grateful to Antonio Sasso for useful and stimulating discussions.

5. Appendix

5.1. Computation of First Two Moments of Photon Count Distribution. Let us assume a single-component solution of chromophores. The treatment given by Chen et al.[25,26] leads to a distribution $\Pi(k,\langle N\rangle)$ of photon counts for an average number $\langle N\rangle$ of molecules in the point spread function volume V_{PSF} of

$$\Pi(k,\langle N\rangle) = \sum_{N=0}^{\infty} \mathrm{Poi}(\langle N\rangle,N)\, P^{(N)}(k) \tag{14}$$

where

$$\mathrm{Poi}(\langle N\rangle,N) = \frac{\langle N\rangle^N}{N!}\exp(-\langle N\rangle)$$

$$P^{(N)}(k) = P^{(1)}(k) \otimes P^{(1)}(k) \otimes \cdots \otimes P^{(1)}(k) \tag{15}$$

$$P^{(1)}(k) = \frac{1}{V_{PSF}}\int \mathrm{d}^3\bar{r}\, \frac{[\epsilon \mathrm{PSF}(\bar{r})]^k}{k!}\exp[-\epsilon \mathrm{PSF}(\bar{r})]$$

The first moment is

$$\langle k\rangle_N = \sum_{k=0}^{\infty} k\Pi(k,\langle N\rangle) = \sum_N \mathrm{Poi}(\langle N\rangle,N)\sum_{k=0}^{\infty} kP^{(N)}(k) \tag{16}$$

where

$$\sum_{k=0}^{\infty} kP^{(N)}(k) = \sum_{k=0}^{\infty} k \prod_{r_1+r_2+\cdots+r_N=k} P^{(1)}(r_1)\, P^{(1)}(r_2) \cdots P^{(1)}(r_N)$$

$$= \sum r_1 P^{(1)}(r_1)\sum_{r_2} P^{(1)}(r_2)\cdots\sum_{r_N} P^{(1)}(r_N) + \cdots + \sum_{r_1} P^{(1)}(r_1)\sum_{r_2} P^{(1)}(r_2)\cdots\sum_{r_N} r_N P^{(1)}(r_N) \tag{17}$$

$$= N\sum_{r_1} r_1 P^{(1)}(r_1)$$

The moment of the single-molecule distribution is

$$\sum_{k=0}^{\infty} kP^{(1)}(k) = \frac{1}{V_{PSF}}\int d^3\bar{r} \sum_{k=0}^{\infty} e^{[-\epsilon PSF(\bar{r})]} k \frac{[\epsilon PSF(\bar{r})]^k}{k!}$$

$$= \frac{1}{V_{PSF}}\int d^3\bar{r}\, e^{[-\mu(\bar{r})]}\mu(\bar{r}) \sum_{k=0}^{\infty} \frac{\partial}{\partial\mu(\bar{r})} \frac{[\mu(\bar{r})]^k}{k!}\Big|_{\mu(\bar{r})=\epsilon PSF(\bar{r})}$$

$$= \frac{1}{V_{PSF}}\int d^3\bar{r}\, \epsilon PSF(\bar{r}) = \epsilon \qquad (18)$$

because $V_{PSF} = \int d^3\bar{r}\, PSF(\bar{r})$. By substituting eqs 17 and 18 into eq 16, we obtain

$$\langle k\rangle_N = \sum_{N=0}^{\infty} Poi(\langle N\rangle, N) N\epsilon = \langle N\rangle\epsilon \qquad (19)$$

For the second moment of the distribution, we first observe that

$$\sum_{k=0}^{\infty} k^2P^{(N)}(k) = N[\sum_{k=0}^{\infty} k^2P^{(1)}(k)] + N(N-1)[\sum_{k=0}^{\infty} kP^{(1)}(k)]^2$$

$$= N(\epsilon + \xi\epsilon^2) + N(N-1)\epsilon^2 \qquad (20)$$

because the second moment of the single-molecule distribution is

$$\sum_{k=0}^{\infty} k^2P^{(1)}(k) = \frac{1}{V_{PSF}}\int d^3\bar{r} \sum_{k=0}^{\infty} e^{[-\epsilon PSF(\bar{r})]} k^2 \frac{[\epsilon PSF(\bar{r})]^k}{k!}$$

$$= \frac{1}{V_{PSF}}\int d^3\bar{r}\, e^{[-\mu(\bar{r})]} \sum_{k=0}^{\infty}\left[\mu(\bar{r}) \frac{\partial}{\partial\mu(\bar{r})}\right]^2 \frac{[\mu(\bar{r})]^k}{k!}\Big|_{\mu(\bar{r})=\epsilon PSF(\bar{r})}$$

$$= \frac{1}{V_{PSF}}\int d^3\bar{r}\, [\epsilon PSF(\bar{r}) + \epsilon^2 PSF(\bar{r})^2] = \epsilon + \xi\epsilon^2 \qquad (21)$$

where

$$\xi = \frac{\int d\bar{r}^3\, [PSF(\bar{r})]^2}{\int d\bar{r}^3\, PSF(\bar{r})} \qquad (22)$$

Then, by averaging over the Poisson distribution of the number of molecules, we obtain

$$\langle k^2\rangle_N = \sum_{N=0}^{\infty} Poi(\langle N\rangle, N) \sum_{k=0}^{\infty} k^2P^{(N)}(k)$$

$$= \langle N\rangle(\epsilon + \xi\epsilon^2) + \langle N^2\rangle\epsilon^2 - \langle N\rangle\epsilon^2 \qquad (23)$$

$$= \langle N\rangle(\epsilon + \xi\epsilon^2) + \langle k\rangle_N^2$$

The Q factor is then

$$Q = \frac{\langle \Delta k^2\rangle_N}{\langle k\rangle_N} = 1 + \xi\epsilon \qquad (24)$$

5.2. Relaxation Time of the Autocorrelation Function for Biased Brownian Motion. We perform here the computation of the autocorrelation function of the fluorescence fluctuations in the presence of a small perturbing potential induced by the light intensity $I(r) = I_0 i(r)$ [with $i(0) = 1$]

$$U(r) = -\frac{n_m^2}{2c\epsilon_r\epsilon_0}\alpha I_0 i(r) = -(\gamma K_B T) i(r) \qquad (25)$$

where $\gamma = \alpha I_0 n_m^2/(2c\epsilon_0\epsilon_r K_B T)$. In terms of the power impinging on the sample, $P = I_0(\pi w_0^2/2)$, the minimum in the trapping potential is

$$U_{min} = -\frac{n_m^2}{2c\epsilon_r\epsilon_0(\pi w_0^2/2)}\alpha P = -uP \qquad (26)$$

For comparisons with the experimental findings, we note that $\gamma = uP/(K_B T)$. For the intensity profile, we assume the form

$$i(r) = \exp[-2(x^2 + y^2)/w_0^2] \exp(-2z^2/z_0^2) \qquad (27)$$

which is the 3-D Gaussian approximation.[31] Throughout the rest of the treatment, we approximate at first order in the amplitude of the interaction potential γ. The fluorescence signal can be written simply as

$$F(t) \propto \sum_{\alpha=1}^{N} \mathcal{M}_\alpha(t)$$

where $\mathcal{M}_\alpha(t)$ is the instantaneous photon fluorescence flux arriving at the detector for each of the N molecules. For an ideal solution of a single species, we can write

$$\langle F(s)\rangle = \mathcal{E}\langle N\rangle\langle \mathcal{M}(s)\rangle = \mathcal{E}\langle N\rangle \int_V d^3\bar{r}\, P(\bar{r})\, I(\bar{r})$$

where the probability of finding a fluorescence particle in $\bar{r}$ depends on the trapping potential according to

$$P(\bar{r}) = A_N^{-1} \exp[-U(\bar{r})/K_B T] \qquad (28)$$

$\mathcal{E}$ is a factor that takes into account the molecular quantum yield and the cross section and instrumental factors, and the average number of molecules in the integration volume V is $\langle N\rangle$. The integration is performed on a closed volume V that we assume to be much larger than the excitation volume $V_{exc} = \int_V i(\bar{r})\, d\bar{r} \approx (\pi/2)^{1.5} w_0^2 z_0$. The normalization factor is

$$A_N = \int_V d^3\bar{r} \exp[-U(\bar{r})/K_B T] \approx V\left(1 + \gamma\frac{V_{exc}}{V}\right) \approx V \qquad (29)$$

as we assume $V_{exc}/V \ll 1$ in the computations. In the previous equation, we have expanded the Boltzmann exponential because we assume that $\gamma \ll 1$.

The fluorescence correlation for an ideal solution is[36]

$$G(t) = \langle F(t+s)\, F(s)\rangle_s \approx \mathcal{E}^2\langle N\rangle\langle \mathcal{M}_\alpha(t+s)\, \mathcal{M}_\alpha(s)\rangle_s \qquad (30)$$

and the autocorrelation of the fluorescence photon flux is

$$\langle \mathcal{M}_\alpha(t+s)\, \mathcal{M}_\alpha(s)\rangle_s = \int d\bar{r}_s\, P(\bar{r}_s) \int d\bar{r}_{s+t} \mathcal{P}(\bar{r}_{t+s}, \bar{r}_s; t)\, i(\bar{r}_s)\, i(\bar{r}_{t+s}) \qquad (31)$$

The conditional probability $\mathcal{A}(\bar{r}_{t+s} - \bar{r}_s, t)$ for the case of the potential given in eq 25 is not easy to compute. To simplify

the computation, we could expand the trapping potential $U(r) \approx -\gamma K_B T + 2\gamma K_B T(x^2 + y^2)/w_0^2 + 2\gamma K_B T z^2/z_0^2$. By expanding $U(r)$ to obtain a harmonic potential, we can write the Smoluchowski equation for the conditional probability[37] as

$$\frac{\partial}{\partial \tau}\mathscr{P}(\bar{r},\tau) = D\frac{\partial^2}{\partial r^2}\mathscr{P}(\bar{r},\tau) + \gamma\bar{\Gamma}\frac{\partial}{\partial \bar{r}}[\bar{r}\mathscr{P}(\bar{r},\tau)] \quad (32)$$

where $\Gamma_x = \Gamma_y = \tau_{xy}^{-1} = 4D/w_0^2$ and $\Gamma_z = \tau_z^{-1} = 4D/z_0^2$. The solution for this equation has been known since the work by Uhlenbeck et al. (1930) to be

$$\mathscr{P}(\bar{r}_{t+s},\bar{r}_s;t) = \frac{\exp[-|\bar{r}_{t+s} - \bar{r}_s A(t)|^2/2B(t)]}{[2\pi B(\tau)]^{0.5}} \quad (33)$$

where $B(t) = [w_0^2/(4\gamma)][1 - \exp(-8\gamma Dt/w_0^2)]$ and $A(t) = \exp(-4\gamma Dt/w_0^2)$.

However, the harmonic approximation of the trapping potential is valid only for high trapping forces, $\gamma \gg 1$, that correspond to the particle moving only in a volume very close to the maximum of the intensity profile. In contrast, small trapping potentials corresponds to $\gamma \approx 0$ and to a wide potential well. In such a case, the particle motion is not restricted to a region close to the maximum of the intensity profile, and the harmonic approximation of the potential around the origin is questionable.

In fact, the direct computation of the normalized autocorrelation function according to

$$g_F(t) = \frac{G(t)}{\langle F(s)\rangle_s^2} = \frac{\langle N\rangle \int d\bar{r}_s\, P(\bar{r}_s) \int d\bar{r}_{t+s}\, \mathscr{P}(\bar{r}_{t+s},\bar{r}_s;t)\, i(\bar{r}_s)\, i(\bar{r}_{t+s})}{[\langle N\rangle \int d\bar{r}_s\, P(\bar{r}_s)\, i(\bar{r}_s)]^2} \quad (34)$$

for the harmonic approximation would lead to a faster relaxation, as shown briefly in the following. The denominator of this equation can be computed in direct space

$$\langle F(s)\rangle_s \approx \mathscr{C}C\int_V d\bar{r}\,[1 + \gamma i(\bar{r})]i(\bar{r}) = \mathscr{C}CV_{exc}(1 + \gamma\xi) \quad (35)$$

where

$$\xi = \frac{\int i(\bar{r})^2\, d\bar{r}}{\int i(\bar{r})\, d\bar{r}} = 2^{-1.5} \quad (36)$$

and C is the number concentration of the solution.

By expanding the probability $P(\bar{r}) \approx 1 + \gamma i(\bar{r})$ to first order in γ, we can write the numerator of eq 34 as

$$g_F(t) \approx \frac{G_0(t) + \gamma\delta G(t)}{\langle F(s)\rangle_s^2} \quad (37)$$

where

$$G_0(t) = \frac{\mathscr{C}^2 CV_{exc}\xi}{(1 + t/\tau_{xy})(1 + t/\tau_z)^{0.5}} \quad (38)$$

The correction to first order in γ is given by

$$\delta G(t) = \int d\bar{r}_s \int d\bar{r}_{t+s} \frac{\exp[-|\bar{r}_{t+s} - \bar{r}_s A(t)|^2/2B(t)]}{[2\pi B(t)]^{0.5}} i(\bar{r}_s)^2\, i(\bar{r}_{t+s}) \quad (39)$$

The higher orders of the expansion of the probability $P(\bar{r})$ would lead to terms of the type

$$\delta G_k(t) = \int d\bar{r}_s \int d\bar{r}_{t+s} \frac{\exp[-|\bar{r}_{t+s} - \bar{r}_s A(t)|^2/2B(t)]}{[2\pi B(t)]^{0.5}} i(\bar{r}_s)^{(1+k)}\, i(\bar{r}_{t+s}) \quad (40)$$

The above integral can be computed easily to give

$$\delta G_k(t) = \frac{\mathscr{C}^2 CV_{exc}\xi(1 + k/2)^{-1.5}}{[1 + 2(1 + k)/(2 + k)t/\tau_{xy}][1 + 2(1 + k)/(2 + k)t/\tau_z]^{0.5}} \quad (41)$$

From this equation, we can see that all of the terms due to the expansion of the probability $P(\bar{r})$ correspond to faster relaxations with characteristic times $\tau_k = \tau_{xy}(2 + k)/(2 + 2k) < \tau_{xy}$. It is easy to demonstrate that the global relaxation of $G(t)$ is therefore faster than that of $G_0(t)$, which is unphysical for Brownian motion in a trapping potential.

We suggest that the origin of this flaw lies in the lack of validity of the expansion of the trapping potential for $\gamma \ll 1$. In this case, we can expand the probability $P(\bar{r}) \approx 1 + \gamma i(\bar{r}) + ...$ to first order in γ. However, the expansion of the Gaussian profile to first order in $\bar{r}$ is not justified because the Brownian particle can span a wide region around the origin. We should therefore use the Smoluchowski equation for the exact trapping potential $U(\bar{r}) = -(\gamma K_B T)i(\bar{r})$

$$\frac{\partial}{\partial t}\mathscr{P}(\bar{r},\tau) = D\frac{\partial^2}{\partial r^2}\mathscr{P}(\bar{r},t) + \gamma\bar{\Gamma}\frac{\partial}{\partial \bar{r}}[\bar{r}i(\bar{r})\,\mathscr{P}(\bar{r},t)] \quad (42)$$

which can be written in Fourier space as

$$\frac{\partial}{\partial t}\hat{\mathscr{P}}(\bar{Q},t) = -DQ^2\hat{\mathscr{P}}(\bar{Q},t) - \frac{1}{2\pi}\gamma(\bar{\Gamma}:\bar{Q})\frac{\partial}{\partial \bar{Q}}[\hat{i}(\bar{Q}) \otimes \hat{\mathscr{P}}(\bar{Q},t)] \quad (43)$$

where

$$\hat{f}(\bar{Q}) = \int_{R^3} f(\bar{r}) \exp(-j\bar{Q}\bar{r})\, d\bar{r}$$
$$f(\bar{r}) = \frac{1}{(2\pi)^3}\int_{R^3} \hat{f}(\bar{Q}) \exp(j\bar{Q}\bar{r})\, d\bar{Q} \quad (44)$$

and $(\bar{\Gamma}:\bar{Q})_\alpha = \Gamma_\alpha Q_\alpha$ for $\alpha = x, y$, and z. The solution of eq 43 for the case $\gamma = 0$ is

$$\hat{P}_0(Q,\tau) = \exp(-Q^2 D\tau) \quad (45)$$

and the Fourier transform of the laser profile is

$$\hat{i}(Q) = V_{exc} \exp[-Q_{xy}^2 w_0^2/8 - Q_z^2 z_0^2/8] \quad (46)$$

where $Q_{xy}^2 = Q_x^2 + Q_y^2$. The solution of eq 43 is not needed for the computation of the average relaxation time of the autocorrelation function defined as $G(\tau) = G(0)/2$. For unper-

turbed Brownian motion in one dimension, we can rewrite τ_0 as

$$\frac{1}{\tau_0} = -\frac{2}{G_0(0)}\frac{\partial}{\partial t}G_0(t)|_{t=0} \tag{47}$$

or

$$\frac{1}{\tau_0} = -\frac{2^{5/2}}{G_0(0)}\frac{\partial}{\partial t}G_0(t)|_{t=\tau_0} \tag{48}$$

In the following, we will find it more convenient to generalize eq 48 to a definition of τ as

$$\frac{1}{\tau} \approx -\frac{2^{5/2}}{G(0)}\frac{\partial}{\partial t}G(t)|_{t=\tau_0} \tag{49}$$

To compute the right-hand term of eq 49, we can write in Fourier space

$$\frac{\partial}{\partial t}G(\tau) = N\int \mathrm{d}^3\bar{Q}\,\frac{\partial}{\partial t}\widehat{\mathscr{P}}(\bar{Q},\tau)\,\hat{\imath}(\bar{Q})\,\widehat{\mathscr{T}}^*(\bar{Q}) \tag{50}$$

where $\hat{\mathscr{T}}(\bar{Q})$ is

$$\widehat{\mathscr{T}}(\bar{Q}) = \int_V \mathrm{d}^3\bar{r}\,\exp(-i\bar{Q}\underline{r})P(\bar{r})\,i(\bar{r}) \approx \int_V \mathrm{d}\bar{r}\,\exp(-i\bar{Q}\bar{r})[i(\bar{r}) + \gamma i(\bar{r})^2] \tag{51}$$

$$\approx \frac{1}{V}[\hat{\imath}(\bar{Q}) + \gamma[V_{\mathrm{exc}}\hat{\imath}(\bar{Q})/2]^{0.5}]$$

to first order in the potential amplitude. We now compute the time derivative of the conditional probability from eq 43 to first order in γ by assuming $\hat{\mathscr{P}}\ (Q,\tau) \approx \widehat{\mathscr{P}_0}(Q,\tau) = \exp(-Q^2D\tau)$ in the computation of the second term on the right-hand side of eq 43 and obtain

$$\frac{\partial}{\partial\tau}\widehat{\mathscr{P}}(Q,\tau) \approx -DQ^2\widehat{\mathscr{P}}_0(Q,\tau) + \frac{2D\gamma {Q_{xy}}^2}{(1+2\tau/\tau_{xy})^{1.5}}\frac{\tau}{\tau_{xy}}\exp\left(-\frac{{Q_{xy}}^2D\tau}{1+2\tau/\tau_{xy}}\right) + \frac{2D\gamma {Q_z}^2}{(1+2\tau/\tau_z)^{1.5}}\frac{\tau}{\tau_z}\exp\left(-\frac{{Q_z}^2D\tau}{1+2\tau/\tau_z}\right) \tag{52}$$

The correlation function at zero delay time can be computed from the relation

$$G(0) = N\int \mathrm{d}\bar{r}_s \int \mathrm{d}\bar{r}_{t+s}\,P(\bar{r}_t)\,i(\bar{r}_t)\,i(\bar{r}_{t+s})\,\delta(\bar{r}_s - \bar{r}_{t+s}) = CV_{\mathrm{exc}}(1+\gamma/2) \tag{53}$$

By substituting eqs 51 and 52 into eq 50, we obtain an expression for the time derivative of the correlation function $G(t)$, which, inserted into eq 49 together with the expression for $G(0)$ in eq 53, leads to an approximation of τ to first order in γ as

$$\frac{1}{\tau} \approx \frac{1}{\tau_0(1+\gamma/2)} + \left(\frac{2}{3}\right)^{1.5}\frac{2\gamma}{\tau_0(1+\gamma/2)} - \left(\frac{2}{3}\right)^{-1.5}\frac{2\gamma}{\tau_0(1+\gamma/2)} \tag{54}$$

$$= \frac{1}{\tau_0(1+\gamma/2)}\left[1 + 2\gamma\left(\frac{2}{3}\right)^{1.5} - 2\gamma\left(\frac{2}{3}\right)^{-1.5}\right]$$

The relaxation time of $G(t)$ is therefore

$$\tau \approx \tau_0(1 + 0.114\gamma) \tag{55}$$

The diffusion time therefore depends linearly on the maximum amplitude of the trapping potential. In the present approximation for a 3-D Gaussian profile, we find that the slope of the relaxation time of the potential is relatively low, ~0.1. This factor should depend on the type of approximation adopted for the intensity profile.

We notice here that the primary approximations used to solve eq 43, are $\hat{\mathscr{P}}(Q,\tau) \approx \widehat{\mathscr{P}_0}(Q,\tau)$ and $P(\bar{r}) = 1 + \gamma i(\bar{r})$. It is worth noting that the present treatment leads to the property that the first-order contribution of the trapping potential to τ at $t = 0$ (see eq 47) vanishes. The solution, eq 55, must be taken cautiously, although it is probably a first attempt at the treatment of a nonharmonic trapping potential.

The average number of molecules can be derived from eqs 53 and 35 as

$$\langle N\rangle = \frac{1}{g_{\mathrm{F}}(0)} = \frac{\langle F(t)\rangle_{\mathrm{t}}^2}{G(0)} = CV_{\mathrm{exc}}[1 + \gamma(2\xi - {}^1/_2)] \approx CV_{\mathrm{exc}}\,[1 + (2\xi - {}^1/_2)(1 - \mathrm{e}^{-\gamma})] \tag{56}$$

This expression is compatible with eq 13 assumed in the text, $N_{\mathrm{obs}} = N_0 + A[1 - \exp(-uP/KT)]$, as $\gamma \approx (1 - \mathrm{e}^{-\gamma})$, and we can therefore write

$$N \approx CV_{\mathrm{exc}}\,[1 + (2\xi - 1/2)(1 - \mathrm{e}^{-\gamma})] \tag{57}$$

References and Notes

(1) Gannaway, J. N.; Sheppard, C. J. R. Second harmonic imaging in the scanning optical microscope. *Opt. Quantum Electron.* **1978**, *10*, 435−439.

(2) Sheppard, C. J. R.; Kompfner, R. Resonant scanning optical microscope. *Appl. Opt.* **1978**, *17*, 2879−2885.

(3) Denk, W.; Strickler, J. H.; Webb, W. W. Two-photon laser scanning fluorescence microscopy. *Science* **1990**, *248*, 73−76.

(4) Wilson, T.; Sheppard, C. J. R. *Theory and Practice of Scanning Optical Microscopy*; Academic Press: London, 1984.

(5) Webb, R. H. Confocal Optical Microscopy. *Rep. Prog. Phys.* **1996**, *59*, 427−471.

(6) Denk, W. Two-photon excitation in functional biological imaging. *J. Biomed. Opt. 1* **1996**, 296−304.

(7) Centonze, V. E.; White, J. G. Multiphoton excitation provides optical sections from deeper within scattering specimens than confocal imaging. *Biophys. J.* **1998**, *75*, 2015−2024.

(8) Magde, D.; Elson, E. L. Fluorescence correlation spectroscopy. II. An experimental realization. *Biopolymers* **1974**, *13*, 29−61.

(9) Elson, E. L.; Magde, D. Fluorescence correlation spectroscopy. I. conceptual basis and theory. *Biopolymers* **1974**, *13*, 1−27.

(10) Thompson, N. Fluorescence Correlation Spectroscopy. In *Topics in Fluorescence Spectroscopy*; Lakowitz, J. R., Ed.; Plenum Press: New York, 1991; Vol. I, Techniques.

(11) Schwille, P.; Bieschke, J.; Oehlenschläger, F. Kinetic investigation by fluorescence correlation spectroscopy: The analytical and diagnostic potential of diffusion studies. *Biophys. Chem.* **1997**, *66*, 211−228.

(12) Sanchez, E. J.; Novotny, L.; Holtom, G. R.; Xie, X. S. *J. Phys. Chem. A* **1997**, *101* (38), 7019−7023.

(13) Chirico, G.; Cannone, F.; Beretta, S.; Baldini, G.; Diaspro, A. Single-Molecule Studies by Means of the Two-Photon Fluorescence Distribution. *Microsc. Res. Technol.* **2001**, *55*, 359−364.

(14) Berland, K. M.; So, P. T.; Gratton, E. Two-photon fluorescence correlation spectroscopy: Method and application to the intracellular environment. *Biophys. J.* **1995**, *68*, 694−701.

(15) König, K.; Liu, Y.; Sonek, G. J.; Berns, M. W.; Tromberg, B. J. Autofluorescence spectroscopy of optically trapped cells. *Photochem. Photobiol.* **1995**, *62* (5) 830−5.

(16) Buehler, C.; Kim, K. H.; Dong, C. Y.; Masters, B. R.; So, P. T. C. Innovations in two-photon deep tissue microscopy. *IEEE Eng. Med. Biol. Mag.* **1999**, *18* (5), 23−30.

(17) Fisher, W. G.; Watcher, E. A.; Armas, M.; Seaton, C. Titanium: Sapphire Laser as an Excitation Source in Two-Photon Spectroscopy. *Appl. Spectrosc.* **1997**, *51* (2), 218−226.

(18) König, K. Laser tweezers are sources of two-photon excitation. *Cell. Mol. Biol.* **1998**, *44* (5), 721−733.

(19) Ashkin, A. Optical trapping and manipulation of neutral particles using lasers. *Proc. Natl. Acad. Sci. U.S.A.* **1997**, *94* (10), 4853−4860.

(20) Ashkin, A. Forces of a single-beam gradient laser trap on a dielectric sphere in the ray optics regime. *Biophys. J.* **1992**, *61*, 569−582.

(21) Ashkin, A. Forces of a Single-Beam Gradient Laser Trap on a Dielectric Sphere in the Ray Optics Regime. *Methods Cell Biol.* **1998**, *55*, 1−27.

(22) Ashkin, A.; Dziedzic, J. M.; Bjorkholm, J. E.; Chu, S. Observation of a single-beam gradient force optical trap for dielectric particles. *Opt. Lett.* **1986**, *11*, 288−90.

(23) Zemánek, P.; Jonás, A.; Šrámek, L.; Liška, M. *Opt. Commun.* **1998**, *151*, 273−285.

(24) Osborne, M. A.; Balasubramanian, S.; Furey, W. S.; Klenerman, D. Optically Biased Diffusion of Single Molecules Studied by Confocal Fluorescence Microscopy. *J. Phys. Chem. B* **1998**, *102* (17), 3160−3167.

(25) Chen, Y.; Muller, J. D.; So, P. T. C.; Gratton, E. The photon counting histogram in fluorescence fluctuation spectroscopy. *Biophys. J.* **1999**, *77*, 553−567.

(26) Kask, P.; Palo, K.; Ullmann, D.; Gall, K. Fluorescence-intensity distribution analysis and its application in biomolecular detection technology. *Proc. Natl. Acad. Sci. U.S.A.* **1999**, *96*, 13756−13761.

(27) Chirico, G.; Olivini, F.; Beretta, S. Fluorescence Excitation Volume in Two-Photon Microscopy by Autocorrelation Spectroscopy and Photon Counting Histogram. *Appl. Spectrosc.* **2000**, *54* (7), 1084−1090.

(28) Rigler, R.; Mets, U.; Windengren, J.; Kask, P. Fluorescence correlation spectroscopy with high count rate and low background: Analysis of translational diffusion. *Eur. Biophys. J.* **1993**, *22*, 169−175.

(29) Bevington, P. R. *Data Reduction and Error Analysis for the Physical Sciences*; McGraw-Hill, New York, 1992; Chapter 11, p 204.

(30) Press, W. H.; Teukolsky, S. A.; Vetterling, W. T.; Flannery, B. P. *Numerical Recipes in C. The Art of Scientific Computing*, 2nd ed.; Cambridge University Press: New York, 1993.

(31) Windegren, J.; Mets, U.; Rigler, R. Fluorescence Correlation Spectroscopy of Triplet State in Solution: A Theoretical and Experimental Study. *J. Phys. Chem.* **1995**, *99*, 13368.

(32) Bieschke, J.; Giese, A.; Schulz-Schaeffer, W.; Zerr, I.; Poser, S.; Eigen, M.; Kretzschmar, H. Ultrasensitive detection of pathological prion protein aggregates by dual-color scanning for intensely fluorescent targets. *Proc. Natl. Acad. Sci. U.S.A.* **2000**, *97*, 5468−5473.

(33) Eggeling, C.; Widengren, J.; Rigler, R.; Seidel, C. A. M. Photobleaching of fluorescent dyes under conditions used for single molecule detection: Evidence of two-step photolysis. *Anal. Chem.* **1998**, *70*, 2651−2659.

(34) Kerker, M. *The Scattering of Light and Other Electromagnetic Radiation*; Academic Press: New York, 1969.

(35) Widengren, J.; Mets, Ü.; Rigler, R. Fluorescence Correlation Spectroscopy of Triplet States in Solution: A Theoretical and Experimental Study. *J. Phys. Chem.* **1995**, *99*, 13368−13379.

(36) Aragon, S. R.; Pecora, R. Fluorescence correlation spectroscopy as a probe of molecular dynamics. *J. Chem. Phys.* **1976**, *64*, 1791−1803.

(37) *The Theory of Polymer Dynamics*; Doi, M., Edwards, S. F., Eds.; International Series of Monographs on Physics; Clarendon Press: Oxford, U.K., 1986; Chapter 3.

(38) Starchev, K.; Zhang, J.; Buffle, J. Applications of Fluorescence Correlation Spectroscopy—Particle Size Effect. *J. Colloid Interface Sci.* **1998**, *203*, 189−196.